

Observation of the helicity-selection-rule suppressed decay of the χ_{c2} charmonium state

M. Ablikim¹, M. N. Achasov^{9,e}, S. Ahmed¹⁴, X. C. Ai¹, O. Albayrak⁵, M. Albrecht⁴, D. J. Ambrose⁴⁴, A. Amoroso^{49A,49C}, F. F. An¹, Q. An^{46,a}, J. Z. Bai¹, O. Bakina²³, R. Baldini Ferrolì^{20A}, Y. Ban³¹, D. W. Bennett¹⁹, J. V. Bennett⁵, N. Berger²², M. Bertani^{20A}, D. Bettoni^{21A}, J. M. Bian⁴³, F. Bianchi^{49A,49C}, E. Boger^{23,c}, I. Boyko²³, R. A. Briere⁵, H. Cai⁵¹, X. Cai^{1,a}, O. Cakir^{40A}, A. Calcaterra^{20A}, G. F. Cao¹, S. A. Cetin^{40B}, J. Chai^{49C}, J. F. Chang^{1,a}, G. Chelkov^{23,c,d}, G. Chen¹, H. S. Chen¹, J. C. Chen¹, M. L. Chen^{1,a}, S. Chen⁴¹, S. J. Chen²⁹, X. Chen^{1,a}, X. R. Chen²⁶, Y. B. Chen^{1,a}, X. K. Chu³¹, G. Cibinetto^{21A}, H. L. Dai^{1,a}, J. P. Dai^{34,j}, A. Dbeyssi¹⁴, D. Dedovich²³, Z. Y. Deng¹, A. Denig²², I. Denysenko²³, M. Destefanis^{49A,49C}, F. De Mori^{49A,49C}, Y. Ding²⁷, C. Dong³⁰, J. Dong^{1,a}, L. Y. Dong¹, M. Y. Dong^{1,a}, Z. L. Dou²⁹, S. X. Du⁵³, P. F. Duan¹, J. Z. Fan³⁹, J. Fang^{1,a}, S. S. Fang¹, X. Fang^{46,a}, Y. Fang¹, R. Farinelli^{21A,21B}, L. Fava^{49B,49C}, F. Feldbauer²², G. Felici^{20A}, C. Q. Feng^{46,a}, E. Fioravanti^{21A}, M. Fritsch^{14,22}, C. D. Fu¹, Q. Gao¹, X. L. Gao^{46,a}, Y. Gao³⁹, Z. Gao^{46,a}, I. Garzia^{21A}, K. Goetzen¹⁰, L. Gong³⁰, W. X. Gong^{1,a}, W. Gradl²², M. Greco^{49A,49C}, M. H. Gu^{1,a}, Y. T. Gu¹², Y. H. Guan¹, A. Q. Guo¹, L. B. Guo²⁸, R. P. Guo¹, Y. Guo¹, Y. P. Guo²², Z. Haddadi²⁵, A. Hafner²², S. Han⁵¹, X. Q. Hao¹⁵, F. A. Harris⁴², K. L. He¹, F. H. Heinsius⁴, T. Held⁴, Y. K. Heng^{1,a}, T. Holtmann⁴, Z. L. Hou¹, C. Hu²⁸, H. M. Hu¹, T. Hu^{1,a}, Y. Hu¹, G. S. Huang^{46,a}, J. S. Huang¹⁵, X. T. Huang³³, X. Z. Huang²⁹, Z. L. Huang²⁷, T. Hussain⁴⁸, W. Ikegami Andersson⁵⁰, Q. Ji¹, Q. P. Ji¹⁵, X. B. Ji¹, X. L. Ji^{1,a}, L. W. Jiang⁵¹, X. S. Jiang^{1,a}, X. Y. Jiang³⁰, J. B. Jiao³³, Z. Jiao¹⁷, D. P. Jin^{1,a}, S. Jin¹, T. Johansson⁵⁰, A. Julin⁴³, N. Kalantar-Nayestanaki²⁵, X. L. Kang¹, X. S. Kang³⁰, M. Kavatsyuk²⁵, B. C. Ke⁵, P. Kiese²², R. Kliemt¹⁰, B. Kloss²², O. B. Kolcu^{40B,h}, B. Kopf⁴, M. Kornicer⁴², A. Kupsc⁵⁰, W. Kühn²⁴, J. S. Lange²⁴, M. Lara¹⁹, P. Larin¹⁴, H. Leithoff²², C. Leng^{49C}, C. Li⁵⁰, Cheng Li^{46,a}, D. M. Li⁵³, F. Li^{1,a}, F. Y. Li³¹, G. Li¹, H. B. Li¹, H. J. Li¹, J. C. Li¹, Jin Li³², K. Li¹³, K. Li³³, Lei Li³, P. R. Li^{7,41}, Q. Y. Li³³, T. Li³³, W. D. Li¹, W. G. Li¹, X. L. Li³³, X. N. Li^{1,a}, X. Q. Li³⁰, Y. B. Li², Z. B. Li³⁸, H. Liang^{46,a}, Y. F. Liang³⁶, Y. T. Liang²⁴, G. R. Liao¹¹, D. X. Lin¹⁴, B. Liu^{34,j}, B. J. Liu¹, C. X. Liu¹, D. Liu^{46,a}, F. H. Liu³⁵, Fang Liu¹, Feng Liu⁶, H. B. Liu¹², H. H. Liu¹, H. H. Liu¹⁶, H. M. Liu¹, J. Liu¹, J. B. Liu^{46,a}, J. P. Liu⁵¹, J. Y. Liu¹, K. Li³⁹, K. Y. Liu²⁷, L. D. Liu³¹, P. L. Liu^{1,a}, Q. Liu⁴¹, S. B. Liu^{46,a}, X. Liu²⁶, Y. B. Liu³⁰, Y. Y. Liu³⁰, Z. A. Liu^{1,a}, Zhiqing Liu²², H. Loehner²⁵, Y. F. Long³¹, X. C. Lou^{1,a,g}, H. J. Lu¹⁷, J. G. Lu^{1,a}, Y. Lu¹, Y. P. Lu^{1,a}, C. L. Luo²⁸, M. X. Luo⁵², T. Luo⁴², X. L. Luo^{1,a}, X. R. Lyu⁴¹, F. C. Ma²⁷, H. L. Ma¹, L. L. Ma³³, M. M. Ma¹, Q. M. Ma¹, T. Ma¹, X. N. Ma³⁰, X. Y. Ma^{1,a}, Y. M. Ma³³, F. E. Maas¹⁴, M. Maggiora^{49A,49C}, Q. A. Malik⁴⁸, Y. J. Mao³¹, Z. P. Mao¹, S. Marcello^{49A,49C}, J. G. Messchendorp²⁵, G. Mezzadri^{21B}, J. Min^{1,a}, T. J. Min¹, R. E. Mitchell¹⁹, X. H. Mo^{1,a}, Y. J. Mo⁶, C. Morales Morales¹⁴, N. Yu. Muchnoi^{9,e}, H. Muramatsu⁴³, P. Musiol⁴, Y. Nefedov²³, F. Nerling¹⁰, I. B. Nikolaev^{9,e}, Z. Ning^{1,a}, S. Nisar⁸, S. L. Niu^{1,a}, X. Y. Niu¹, S. L. Olsen³², Q. Ouyang^{1,a}, S. Pacetti^{20B}, Y. Pan^{46,a}, P. Patteri^{20A}, M. Pelizaeus⁴, H. P. Peng^{46,a}, K. Peters^{10,i}, J. Pettersson⁵⁰, J. L. Ping²⁸, R. G. Ping¹, R. Poling⁴³, V. Prasad¹, H. R. Qi², M. Qi²⁹, S. Qian^{1,a}, C. F. Qiao⁴¹, L. Q. Qin³³, N. Qin⁵¹, X. S. Qin¹, Z. H. Qin^{1,a}, J. F. Qiu¹, K. H. Rashid⁴⁸, C. F. Redmer²², M. Ripka²², G. Rong¹, Ch. Rosner¹⁴, X. D. Ruan¹², A. Sarantsev^{23,f}, M. Savrie^{21B}, C. Schnier⁴, K. Schoenning⁵⁰, W. Shan³¹, M. Shao^{46,a}, C. P. Shen², P. X. Shen³⁰, X. Y. Shen¹, H. Y. Sheng¹, W. M. Song¹, X. Y. Song¹, S. Sosio^{49A,49C}, S. Spataro^{49A,49C}, G. X. Sun¹, J. F. Sun¹⁵, S. S. Sun¹, X. H. Sun¹, Y. J. Sun^{46,a}, Y. Z. Sun¹, Z. J. Sun^{1,a}, Z. T. Sun¹⁹, C. J. Tang³⁶, X. Tang¹, I. Tapan^{40C}, E. H. Thorndike⁴⁴, M. Tiemens²⁵, I. Uman^{40D}, G. S. Varner⁴², B. Wang³⁰, B. L. Wang⁴¹, D. Wang³¹, D. Y. Wang³¹, K. Wang^{1,a}, L. L. Wang¹, L. S. Wang¹, M. Wang³³, P. Wang¹, P. L. Wang¹, W. Wang^{1,a}, W. P. Wang^{46,a}, X. F. Wang³⁹, Y. Wang³⁷, Y. D. Wang¹⁴, Y. F. Wang^{1,a}, Y. Q. Wang²², Z. Wang^{1,a}, Z. G. Wang^{1,a}, Z. H. Wang^{46,a}, Z. Y. Wang¹, Z. Y. Wang¹, T. Weber²², D. H. Wei¹¹, P. Weidenkaff²², S. P. Wen¹, U. Wiedner⁴, M. Wolke⁵⁰, L. H. Wu¹, L. J. Wu¹, Z. Wu^{1,a}, L. Xia^{46,a}, L. G. Xia³⁹, Y. Xia¹⁸, D. Xiao¹, H. Xiao⁴⁷, Z. J. Xiao²⁸, Y. G. Xie^{1,a}, Y. H. Xie⁶, Q. L. Xiu^{1,a}, G. F. Xu¹, J. J. Xu¹, L. Xu¹, Q. J. Xu¹³, Q. N. Xu⁴¹, X. P. Xu³⁷, L. Yan^{49A,49C}, W. B. Yan^{46,a}, W. C. Yan^{46,a}, Y. H. Yan¹⁸, H. J. Yang^{34,j}, H. X. Yang¹, L. Yang⁵¹, Y. X. Yang¹¹, M. Ye^{1,a}, M. H. Ye⁷, J. H. Yin¹, Z. Y. You³⁸, B. X. Yu^{1,a}, C. X. Yu³⁰, J. S. Yu²⁶, C. Z. Yuan¹, Y. Yuan¹, A. Yuncu^{40B,b}, A. A. Zafar⁴⁸, Y. Zeng¹⁸, Z. Zeng^{46,a}, B. X. Zhang¹, B. Y. Zhang^{1,a}, C. C. Zhang¹, D. H. Zhang¹, H. H. Zhang³⁸, H. Y. Zhang^{1,a}, J. Zhang¹, J. J. Zhang¹, J. L. Zhang¹, J. Q. Zhang¹, J. W. Zhang^{1,a}, J. Y. Zhang¹, J. Z. Zhang¹, K. Zhang¹, L. Zhang¹, S. Q. Zhang³⁰, X. Y. Zhang³³, Y. Zhang¹, Y. Zhang¹, Y. H. Zhang^{1,a}, Y. N. Zhang⁴¹, Y. T. Zhang^{46,a}, Yu Zhang⁴¹, Z. H. Zhang⁶, Z. P. Zhang⁴⁶, Z. Y. Zhang⁵¹, G. Zhao¹, J. W. Zhao¹, J. Y. Zhao¹, J. Z. Zhao^{1,a}, Lei Zhao^{46,a}, Ling Zhao¹, M. G. Zhao³⁰, Q. Zhao¹, Q. W. Zhao¹, S. J. Zhao⁵³, T. C. Zhao¹, Y. B. Zhao^{1,a}, Z. G. Zhao^{46,a}, A. Zhemchugov^{23,c}, B. Zheng^{14,47}, J. P. Zheng^{1,a}, W. J. Zheng³³, Y. H. Zheng⁴¹, B. Zhong²⁸, L. Zhou^{1,a}, X. Zhou⁵¹, X. K. Zhou^{46,a}, X. R. Zhou^{46,a}, X. Y. Zhou¹, K. Zhu¹, K. J. Zhu^{1,a}, S. Zhu¹, S. H. Zhu⁴⁵, X. L. Zhu³⁹, Y. C. Zhu^{46,a}, Y. S. Zhu¹, Z. A. Zhu¹, J. Zhuang^{1,a}, L. Zotti^{49A,49C}, B. S. Zou¹, J. H. Zou¹

(BESIII Collaboration)

¹ Institute of High Energy Physics, Beijing 100049, People's Republic of China

² Beihang University, Beijing 100191, People's Republic of China

³ Beijing Institute of Petrochemical Technology, Beijing 102617, People's Republic of China

⁴ Bochum Ruhr-University, D-44780 Bochum, Germany

⁵ Carnegie Mellon University, Pittsburgh, Pennsylvania 15213, USA

⁶ Central China Normal University, Wuhan 430079, People's Republic of China

⁷ China Center of Advanced Science and Technology, Beijing 100190, People's Republic of China

⁸ COMSATS Institute of Information Technology, Lahore, Defence Road, Off Raiwind Road, 54000 Lahore, Pakistan

⁹ G.I. Budker Institute of Nuclear Physics SB RAS (BINP), Novosibirsk 630090, Russia

¹⁰ GSI Helmholtzcentre for Heavy Ion Research GmbH, D-64291 Darmstadt, Germany

- ¹¹ Guangxi Normal University, Guilin 541004, People's Republic of China
¹² Guangxi University, Nanning 530004, People's Republic of China
¹³ Hangzhou Normal University, Hangzhou 310036, People's Republic of China
¹⁴ Helmholtz Institute Mainz, Johann-Joachim-Becher-Weg 45, D-55099 Mainz, Germany
¹⁵ Henan Normal University, Xinxiang 453007, People's Republic of China
¹⁶ Henan University of Science and Technology, Luoyang 471003, People's Republic of China
¹⁷ Huangshan College, Huangshan 245000, People's Republic of China
¹⁸ Hunan University, Changsha 410082, People's Republic of China
¹⁹ Indiana University, Bloomington, Indiana 47405, USA
²⁰ (A)INFN Laboratori Nazionali di Frascati, I-00044, Frascati, Italy; (B)INFN and University of Perugia, I-06100, Perugia, Italy
²¹ (A)INFN Sezione di Ferrara, I-44122, Ferrara, Italy; (B)University of Ferrara, I-44122, Ferrara, Italy
²² Johannes Gutenberg University of Mainz, Johann-Joachim-Becher-Weg 45, D-55099 Mainz, Germany
²³ Joint Institute for Nuclear Research, 141980 Dubna, Moscow region, Russia
²⁴ Justus-Liebig-Universitaet Giessen, II. Physikalisches Institut, Heinrich-Buff-Ring 16, D-35392 Giessen, Germany
²⁵ KVI-CART, University of Groningen, NL-9747 AA Groningen, The Netherlands
²⁶ Lanzhou University, Lanzhou 730000, People's Republic of China
²⁷ Liaoning University, Shenyang 110036, People's Republic of China
²⁸ Nanjing Normal University, Nanjing 210023, People's Republic of China
²⁹ Nanjing University, Nanjing 210093, People's Republic of China
³⁰ Nankai University, Tianjin 300071, People's Republic of China
³¹ Peking University, Beijing 100871, People's Republic of China
³² Seoul National University, Seoul, 151-747 Korea
³³ Shandong University, Jinan 250100, People's Republic of China
³⁴ Shanghai Jiao Tong University, Shanghai 200240, People's Republic of China
³⁵ Shanxi University, Taiyuan 030006, People's Republic of China
³⁶ Sichuan University, Chengdu 610064, People's Republic of China
³⁷ Soochow University, Suzhou 215006, People's Republic of China
³⁸ Sun Yat-Sen University, Guangzhou 510275, People's Republic of China
³⁹ Tsinghua University, Beijing 100084, People's Republic of China
⁴⁰ (A)Ankara University, 06100 Tandogan, Ankara, Turkey; (B)Istanbul Bilgi University, 34060 Eyup, Istanbul, Turkey; (C)Uludag University, 16059 Bursa, Turkey; (D)Near East University, Nicosia, North Cyprus, Mersin 10, Turkey
⁴¹ University of Chinese Academy of Sciences, Beijing 100049, People's Republic of China
⁴² University of Hawaii, Honolulu, Hawaii 96822, USA
⁴³ University of Minnesota, Minneapolis, Minnesota 55455, USA
⁴⁴ University of Rochester, Rochester, New York 14627, USA
⁴⁵ University of Science and Technology Liaoning, Anshan 114051, People's Republic of China
⁴⁶ University of Science and Technology of China, Hefei 230026, People's Republic of China
⁴⁷ University of South China, Hengyang 421001, People's Republic of China
⁴⁸ University of the Punjab, Lahore-54590, Pakistan
⁴⁹ (A)University of Turin, I-10125, Turin, Italy; (B)University of Eastern Piedmont, I-15121, Alessandria, Italy; (C)INFN, I-10125, Turin, Italy
⁵⁰ Uppsala University, Box 516, SE-75120 Uppsala, Sweden
⁵¹ Wuhan University, Wuhan 430072, People's Republic of China
⁵² Zhejiang University, Hangzhou 310027, People's Republic of China
⁵³ Zhengzhou University, Zhengzhou 450001, People's Republic of China
^a Also at State Key Laboratory of Particle Detection and Electronics, Beijing 100049, Hefei 230026, People's Republic of China
^b Also at Bogazici University, 34342 Istanbul, Turkey
^c Also at the Moscow Institute of Physics and Technology, Moscow 141700, Russia
^d Also at the Functional Electronics Laboratory, Tomsk State University, Tomsk, 634050, Russia
^e Also at the Novosibirsk State University, Novosibirsk, 630090, Russia
^f Also at the NRC "Kurchatov Institute", PNPI, 188300, Gatchina, Russia
^g Also at University of Texas at Dallas, Richardson, Texas 75083, USA
^h Also at Istanbul Arel University, 34295 Istanbul, Turkey
ⁱ Also at Goethe University Frankfurt, 60323 Frankfurt am Main, Germany
^j Also at Key Laboratory for Particle Physics, Astrophysics and Cosmology, Ministry of Education; Shanghai Key Laboratory for Particle Physics and Cosmology; Institute of Nuclear and Particle Physics, Shanghai 200240, People's Republic of China

The decays of $\chi_{c2} \rightarrow K^+ K^- \pi^0$, $K_S K^\pm \pi^\mp$ and $\pi^+ \pi^- \pi^0$ are studied with the $\psi(3686)$ data samples

collected with the Beijing Spectrometer (BESIII). For the first time, the branching fractions of $\chi_{c2} \rightarrow K^* \bar{K}$, $\chi_{c2} \rightarrow a_2^\pm(1320)\pi^\mp/a_2^0(1320)\pi^0$ and $\chi_{c2} \rightarrow \rho(770)^\pm\pi^\mp$ are measured. Here $K^* \bar{K}$ denotes both $K^{*\pm}K^\mp$ and $K^{*0}\bar{K}^0 + c.c.$, and K^* denotes the resonances $K^*(892)$, $K_2^*(1430)$ and $K_3^*(1780)$. The observations indicate a strong violation of the helicity selection rule in χ_{c2} decays into vector and pseudoscalar meson pairs. The measured branching fractions of $\chi_{c2} \rightarrow K^*(892)\bar{K}$ are more than 10 times larger than the upper limit of $\chi_{c2} \rightarrow \rho(770)^\pm\pi^\mp$, which is so far the first direct observation of a significant U -spin symmetry breaking effect in charmonium decays.

PACS numbers: 13.25.Gv, 12.38.Qk

The helicity selection rule (HSR) [1–3] is one of the most important consequences of perturbative quantum chromodynamics (pQCD) at leading twist accuracy. In the charmonium energy region, although there are observations that pQCD plays a dominant role, there are also many hints that non-perturbative mechanisms can become important [3–6]. Exclusive decays of the P -wave charmonium state $\chi_{c2} \rightarrow VP$, where V and P denote light vector and pseudoscalar mesons, respectively, are ideal for testing the HSR and pinning down the mechanisms that may violate the leading pQCD theory.

Another reason the decays of $\chi_{c2} \rightarrow VP$ are of great interest is that this process is ideal for probing the long-range interactions arising from intermediate D -meson loop transitions. As pointed out in Ref. [7], if the intermediate D -meson loops provide the non-perturbative mechanism to violate the HSR, this can be identified by the measurements of $\chi_{c2} \rightarrow K^*(892)\bar{K}$ and $\chi_{c2} \rightarrow \rho(770)^\pm\pi^\mp$. Throughout the text, $K^* \bar{K}$ denotes $K^{*\pm}K^\mp$ and its isospin-conjugated process $K^{*0}\bar{K}^0 + c.c.$, and K^* denotes the resonances $K^*(892)$, $K_2^*(1430)$ and $K_3^*(1780)$. For the $\chi_{c2} \rightarrow K^*(892)\bar{K}$ process, due to U -spin symmetry breaking, a sizeable branching fraction $[(4.0 \sim 6.7) \times 10^{-5}]$ is predicted, while the branching fraction for $\chi_{c2} \rightarrow \rho(770)^\pm\pi^\mp$ is expected to be much smaller [7].

In this Letter, we present a partial wave analysis (PWA) of the process $\chi_{c2} \rightarrow K \bar{K} \pi$ (denotes $K^+K^-\pi^0$ and $K_S K^\pm \pi^\mp$) and a measurement of $\chi_{c2} \rightarrow \pi^+ \pi^- \pi^0$. We have two $\psi(3686)$ samples of $(106.8 \pm 0.8) \times 10^6$ (160 pb^{-1}) [8] and $(341.1 \pm 2.1) \times 10^6$ (510 pb^{-1}) [9] events collected in 2009 and 2012 by BESIII [10], respectively. Only the 2009 data sample is used in the analysis of $\chi_{c2} \rightarrow K \bar{K} \pi$, and the full data sample is used in $\chi_{c2} \rightarrow \pi^+ \pi^- \pi^0$ since it has a smaller branching fraction. An independent sample of about 44 pb^{-1} taken at $\sqrt{s} = 3.65 \text{ GeV}$ is utilized to investigate the potential background from the continuum process. A sample of Monte Carlo (MC) simulated events of generic $\psi(3686)$ decays (‘inclusive MC sample’) is used to study backgrounds. The optimization of the event selection and the estimation of physics backgrounds are performed with Monte Carlo simulations of $\psi(3686)$ inclusive/exclusive decays.

The χ_{c2} candidates, produced in $\psi(3686)$ radiative decays, are reconstructed from the final states $K^+K^-\pi^0$,

$K_S K^\pm \pi^\mp$, and $\pi^+ \pi^- \pi^0$. Each charged track is required to have a polar angle θ in the main drift chamber (MDC) that satisfies $|\cos \theta| < 0.93$, and have the point of closest approach to the e^+e^- interaction point within 10 cm in the beam direction ($|V_z|$), and 1 cm in the plane perpendicular to the beam direction (V_r). The energy loss dE/dx in the MDC and the information from the time-of-flight (TOF) system are combined to form particle identification (PID) confidence levels (C.L.) for the π , K , and p hypotheses, and each track is assigned with the hypothesis corresponding to the highest C.L. The K_S candidates are reconstructed with two oppositely charged tracks with loose vertex requirements ($|V_z| < 30 \text{ cm}$ and $V_r < 10 \text{ cm}$) and without PID (assumed to be pions). Then the candidate with invariant mass closest to the K_S nominal mass and the decay length provided by a secondary vertex fit algorithm greater than 0.25 cm, is selected for further study in the decay $\psi(3686) \rightarrow \gamma K_S K^\pm \pi^\mp$. The candidate events are required to have two charged tracks with zero net charge, where the tracks from the K_S candidate are not taken into account. Two pions and one kaon are required for the decays $\psi(3686) \rightarrow \gamma \pi^+ \pi^- \pi^0$ and $\psi(3686) \rightarrow \gamma K_S K^\pm \pi^\mp$, respectively, and no PID requirement is applied for the decay $\psi(3686) \rightarrow \gamma K^+ K^- \pi^0$. The photon candidates are required to have energy larger than 25 (50) MeV in the Electromagnetic Calorimeter (EMC) barrel (end cap) region $|\cos \theta| < 0.8$ ($0.86 < |\cos \theta| < 0.93$), and have an angle relative to the nearest charged tracks larger than 10° . To suppress electronic noise and energy deposits unrelated to the event, the EMC cluster time must be within 700 ns from the event start time. At least three and one photons are required for the decay $\psi(3686) \rightarrow \gamma \pi^+ \pi^- \pi^0 / K^+ K^- \pi^0$ and $\psi(3686) \rightarrow \gamma K_S K^\pm \pi^\mp$, respectively.

A kinematic fit (4C) enforcing four-momentum conservation between the initial $\psi(3686)$ and the final state is performed for each process. If there are more photons than required in one event, all possible combinations of photons are considered and only the one with the least χ_{4C}^2 of the kinematic fit is retained for further analysis. The χ_{4C}^2 is required to be less than 80 and 60 for the decay $\psi(3686) \rightarrow \gamma K^+ K^- \pi^0$ and $\psi(3686) \rightarrow \gamma K_S K^\pm \pi^\mp$, respectively. The π^0 candidate is reconstructed with the two selected photons whose invariant mass is closest to the π^0 nominal mass, and satisfies $|M_{\gamma\gamma} - M_{\pi^0}| <$

10 MeV/c². For the decay mode $\psi(3686) \rightarrow \gamma\pi^+\pi^-\pi^0$, a 5C kinematic fit is performed with an additional π^0 mass constraint, and $\chi_{5C}^2 < 60$ is required. To remove the backgrounds from the decays $\psi(3686) \rightarrow \pi^0\pi^0 J/\psi$ ($J/\psi \rightarrow l^+l^-$), the invariant mass of $K^+K^-/\pi^+\pi^-$ is required to be less than 3.0 GeV/c² for the decay $\psi(3686) \rightarrow \gamma K^+K^-\pi^0/\gamma\pi^+\pi^-\pi^0$. In the decay mode $\psi(3686) \rightarrow \gamma\pi^+\pi^-\pi^0$, the π^0 recoil mass is required to be less than 3.0 GeV/c² to suppress the background $\psi(3686) \rightarrow \pi^0 J/\psi$, and $M_{\gamma\pi^0} \notin (0.7, 0.85)$ GeV/c² is required to veto the background $\psi(3686) \rightarrow \omega\pi^+\pi^-$ ($\omega \rightarrow \gamma\pi^0$).

The distributions of the $K\bar{K}\pi$ invariant mass for the decay $\psi(3686) \rightarrow \gamma K^+K^-\pi^0$ and $\psi(3686) \rightarrow \gamma K_S K^\pm\pi^\mp$ are shown in Fig. 1(a) and (b), respectively. The $\chi_{c1,2}$ signals appear prominently with a small background. From the analysis of the $\psi(3686)$ inclusive MC sample and the continuum data at $\sqrt{s} = 3.65$ GeV, the main backgrounds are from the decays $\psi(3686) \rightarrow \pi^0\pi^0 J/\psi$ ($J/\psi \rightarrow \pi^+\pi^-\pi^0/\mu\mu$), and $\psi(3686) \rightarrow K_1(1270)^\pm K^\mp$ ($K_1(1270)^\pm \rightarrow K^\pm\pi^0\pi^0/\rho(770)^\pm K_S$). All of these backgrounds show a smooth distribution, and do not produce a peak around the $\chi_{c1,2}$ mass region. Unbinned maximum likelihood fits are performed to the selected candidates, where the $\chi_{c1,2}$ signals are described with the MC simulated shapes convoluted with a Gaussian function accounting for the resolution difference between data and MC simulation, and the backgrounds are described with a 2nd order polynomial function. There are 1215 and 1176 candidate events for $\chi_{c2} \rightarrow K^+K^-\pi^0$ and $\chi_{c2} \rightarrow K_S K^\pm\pi^\mp$ within the χ_{c2} signal region $|M_{K\bar{K}\pi} - M_{\chi_{c2}}| \leq 15$ MeV/c². Non- χ_{c2} and non- π^0 (in the $K^+K^-\pi^0$ mode only) backgrounds are estimated with the events in the sideband regions, which are also used in the PWA as described in the following. The numbers of background events are estimated to be 240 and 80 for $\chi_{c2} \rightarrow K^+K^-\pi^0$ and $\chi_{c2} \rightarrow K_S K^\pm\pi^\mp$, respectively.

To determine the signal yields of the different intermediate states within the process $\chi_{c2} \rightarrow K\bar{K}\pi$, a PWA is performed. The process is assumed to proceed via the quasi two-body decays, *i.e.* $\chi_{c2} \rightarrow a_2\pi$ and $K^*\bar{K}$ followed by $a_2 \rightarrow K^+K^-$ and $K^* \rightarrow K\pi$. The amplitudes of the two-body decays are constructed with the helicity-covariant method [11]. For a particle decaying into two-body final states, *i.e.* $A(J, m) \rightarrow B(s, \lambda)C(\sigma, \nu)$, where spin and helicity are indicated in the parentheses, its helicity covariant amplitude $F_{\lambda, \nu}$ [11] is:

$$F_{\lambda, \nu} = \sum_{lS} A_{gIS} \langle l0S\delta | J\delta \rangle \langle s\lambda\sigma - \nu | S\delta \rangle r^l B_l(r), \quad (1)$$

where $A \equiv \sqrt{\frac{2l+1}{2J+1}}$, g_{IS} is the coupling constant for the partial wave with orbital angular momentum l and spin S (with z -projection δ), r is the relative momentum between the two daughter particles in the initial particle rest frame, and B_l is the barrier factor [12]. The con-

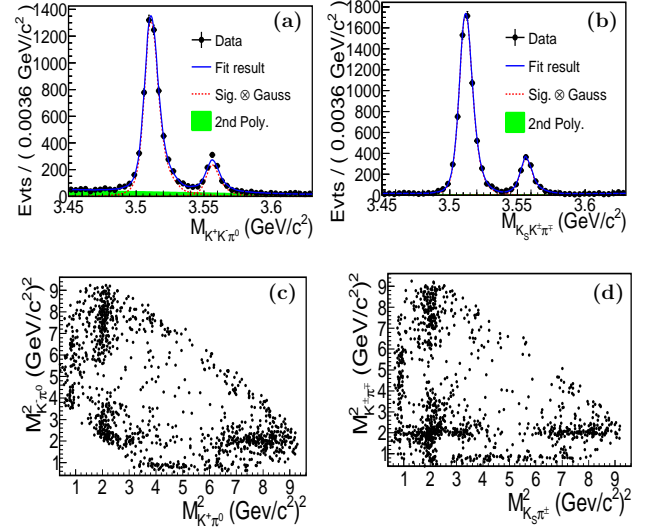


FIG. 1. (color online) Invariant mass distribution of (a) $K^+K^-\pi^0$ and (b) $K_S K^\pm\pi^\mp$ for the decay $\psi(3686) \rightarrow \gamma K\bar{K}\pi$, and the corresponding Dalitz distributions (c) and (d) for the candidates within $|M_{K\bar{K}\pi} - M_{\chi_{c2}}| < 15$ MeV/c². The dots with error bars are for data, the blue solid curves are the overall fit results, the red dotted curves are the signals, and the green shaded areas are the background.

servation of parity is applied in the equation. Recent measurements show that the contributions of higher order magnetic and electric multipoles in the $\psi(3686)$ radiative transition to χ_{c2} are negligible, and the $E1$ transition is the dominant process [13]. Hence, the helicity amplitudes are constructed to satisfy the $E1$ transition relation [14] and parity conservation, namely, $F_{1,2} = \sqrt{2}F_{1,1} = \sqrt{6}F_{1,0}$ and $F_{0,0} = 0$. The corresponding g_{IS} are taken as complex values. The relative magnitudes and phases are determined by an un-binned maximum likelihood fit to data with the package MINUIT [15]. The background contribution to the likelihood value is estimated with the events in the sideband regions, and is subtracted, as done in Ref. [16]. The Input/Output check has been performed for the analysis method, and the output result shows consistent with that of the input.

As shown in the Dalitz plots of Fig. 1(c) and (d), clear signals for $K^*(892)$ and $K_2^*(1430)$ are observed in the $K\pi$ system. Other possible excited K^* states in $K\pi$ system and the states in the $K\bar{K}$ system listed in PDG [17] are considered in the fit, and their statistical significances are estimated with the difference of likelihood values between the fits with and without the corresponding components included, and taking into account the change of the number of degrees of freedom. The resonances $K^*(892)$ and $K_2^*(1430)$ in the $K\pi$ system as well as the $a_2(1320)$ in the $K\bar{K}$ system, which has a statistical significance larger than 8σ in both decay modes, are included in the baseline solution. For consistency, the $K_3^*(1780)$ signal, which is of a significance larger than 5σ in the decay

$\chi_{c2} \rightarrow K_S K^\pm \pi^\mp$, but only 2σ in $\chi_{c2} \rightarrow K^+ K^- \pi^0$, is also included. A contribution from the direct $\chi_{c2} \rightarrow K \bar{K} \pi$ three-body decay, which is parameterized with a non-resonant component with spin-parity $J^P = 2^+$ in the $K \bar{K}$ system, is also considered. Other possible intermediate states, which have a statistical significance less than 5σ , are not included. They are considered as a source of systematic uncertainty. The coupling constants for the charge-conjugate modes are treated to be the same.

Figures 2 and 3(a)-(c) show the invariant mass distribution and the projection of the PWA for the decays $\chi_{c2} \rightarrow K^+ K^- \pi^0$ and $\chi_{c2} \rightarrow K_S K^\pm \pi^\mp$, respectively. The signal yields for the individual processes with a given intermediate state and the corresponding statistical uncertainties are calculated according to the fit results. The resultant branching fractions for the decays $\chi_{c2} \rightarrow K^* \bar{K}$ and $\chi_{c2} \rightarrow a_2(1320)\pi$ are summarized in Table I. The branching fractions for the processes including charged K^* intermediate states are consistent between the two decay modes, and are combined by considering the correlation of uncertainties between the two modes [18]. The results are also summarized in Table I. The measured branching fractions are at the level of 10^{-4} , and the K^* isospin-conjugate modes are consistent with each other within 2σ , as expected by isospin symmetry.

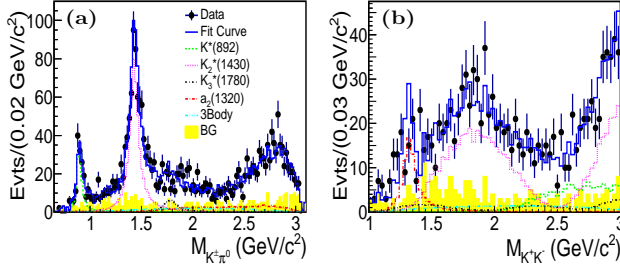


FIG. 2. (color online) Projections of the fit results onto the invariant mass of (a) $K^\pm \pi^0$ and (b) $K^+ K^-$ in the decay $\chi_{c2} \rightarrow K^+ K^- \pi^0$, where dots with error bars are for data, the blue solid histograms are the overall fit results, the yellow shaded histograms are for the background estimated using χ_{c2} sideband events, and the contributions from different components are indicated in the inset.

The large branching ratio of $\chi_{c2} \rightarrow K_2^* \bar{K}$ is a direct indication of the significant HSR violation effects. Note that the helicity amplitude ratios $|F_{2,0}|^2/|F_{1,0}|^2$, estimated with the fitted g_{IS} (see Table II), suggest the dominance of $F_{1,0}$ in the transition amplitudes. The amplitude $F_{1,0}$ contributes to the leading HSR violation effects and scales as $(\Lambda_{QCD}/m_c)^6$ due to its asymptotic behavior [2, 7]. In comparison with the HSR conserved channel $\chi_{c2} \rightarrow VV$, which scales as $(\Lambda_{QCD}/m_c)^4$, the ratio of $\chi_{c2} \rightarrow K_2^* \bar{K}$ to VV is expected to be suppressed by a factor of $(\Lambda_{QCD}/m_c)^2 \sim 0.02$ with $\Lambda_{QCD} \sim 0.2$ GeV/ c^2 and the charm quark mass $m_c \sim 1.5$ GeV/ c^2 . However, the measured branching fraction of $\chi_{c2} \rightarrow K_2^* \bar{K}$ appears to be the same order of magnitude as that for

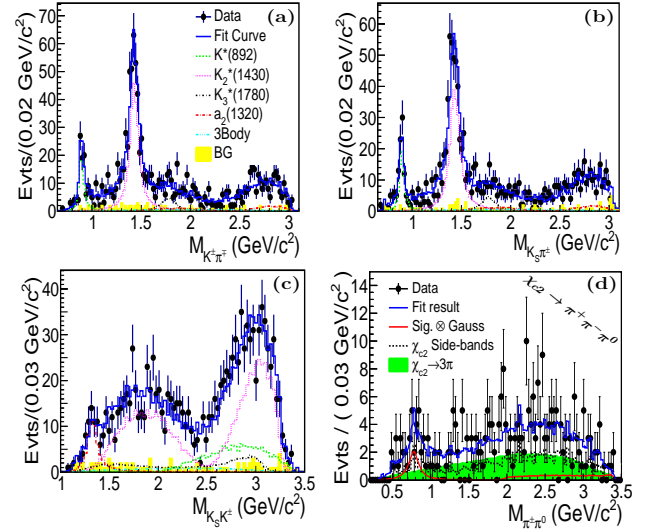


FIG. 3. (color online) Projections of the fit results onto the invariant mass of (a) $K^\pm \pi^\pm$, (b) $K_S \pi^\pm$ and (c) $K_S K^\pm$ in the decay $\chi_{c2} \rightarrow K_S K^\pm \pi^\mp$ as well as (d) $\pi^\pm \pi^0$ in the decay $\chi_{c2} \rightarrow \pi^\pm \pi^0 \pi^0$, where dots with error bars are for data, the blue solid histograms are the overall fit results, and the contributions from other components are indicated in the inset.

TABLE I. The measured branching fractions ($\times 10^{-4}$) for the decays $\chi_{c2} \rightarrow (K\pi)\bar{K}$ and $\chi_{c2} \rightarrow (K\bar{K})\pi$. The first uncertainties are statistical, and the second are systematic (Here, K^* , K_2^* , K_3^* , and a_2 refer to $K^*(892)$, $K_2^*(1430)$, $K_3^*(1780)$, and $a_2(1320)$, respectively).

Mode	$K^+ K^- \pi^0$	$K_S K^\pm \pi^\mp$	Combined
$K^{*\pm} K^\mp$	$1.8 \pm 0.2 \pm 0.2$	$1.4 \pm 0.2 \pm 0.2$	$1.5 \pm 0.1 \pm 0.2$
$K^{*0} \bar{K}^0$	—	$1.3 \pm 0.2 \pm 0.2$	—
$K_2^{*\pm} K^\mp$	$18.2 \pm 0.8 \pm 1.6$	$13.6 \pm 0.8 \pm 1.4$	$15.5 \pm 0.6 \pm 1.2$
$K_2^{*0} \bar{K}^0$	—	$13.0 \pm 1.0 \pm 1.5$	—
$K_3^{*\pm} K^\mp$	$5.3 \pm 0.5 \pm 0.9$	$5.9 \pm 1.1 \pm 1.5$	$5.4 \pm 0.5 \pm 0.7$
$K_3^{*0} \bar{K}^0$	—	$5.9 \pm 1.6 \pm 1.5$	—
$a_2^0 \pi^0$	$13.5 \pm 1.6 \pm 3.2$	—	—
$a_2^\pm \pi^\mp$	—	$18.4 \pm 3.3 \pm 5.5$	—

$\chi_{c2} \rightarrow VV$ [19], which indicates a significant violation of HSR in $\chi_{c2} \rightarrow K_2^* \bar{K}$.

TABLE II. The measured ratios of helicity amplitude squared $|F_{2,0}|^2/|F_{1,0}|^2$, where the uncertainties are statistical only.

	$K^+ K^- \pi^0$	$K_S K^\pm \pi^\mp$
	Charged K^*	Charged K^* Neutral K^*
$K_2^*(1430)$	0.046 ± 0.001	0.042 ± 0.019 0.031 ± 0.018

In the analysis of the decay $\psi(3686) \rightarrow \gamma \pi^+ \pi^- \pi^0$, the χ_{c2} signal is extracted by the requirement $|M_{\pi^+ \pi^- \pi^0} - M_{\chi_{c2}}| \leq 15$ MeV/ c^2 . The potential background from direct $e^+ e^-$ annihilation is found to be negligible by studying the continuum data taken at $\sqrt{s} = 3.65$ GeV. The backgrounds from $\psi(3686)$ decay are investigated

with the $\psi(3686)$ inclusive MC sample; the only surviving χ_{c2} events are those that directly decay to $\pi^+\pi^-\pi^0$ without any intermediate state. There are also non- χ_{c2} backgrounds, which can be estimated by the events in the χ_{c2} sideband regions. Figure 3(d) shows the invariant mass of $\pi^\pm\pi^0$ for the selected candidates, together with the binned likelihood fit results. Here the fit components include the $\rho(770)^\pm$ signal, the direct decay $\chi_{c2} \rightarrow \pi^+\pi^-\pi^0$ and the non- χ_{c2} background. The $\rho(770)^\pm$ signal and the direct χ_{c2} three-body decay are modeled with the MC simulated shapes convoluted with a Gaussian function with free parameters which accounts for the resolution difference between data and MC simulation. The resonant parameters of the $\rho(770)^\pm$ are set to the values in the PDG [17]. The fitted signal yields are 14.7 ± 8.9 and 63.6 ± 13.0 , and the corresponding resultant branching fractions are $(0.64 \pm 0.39 \pm 0.07) \times 10^{-5}$ and $(2.1 \pm 0.4 \pm 0.2) \times 10^{-5}$ for $\chi_{c2} \rightarrow \rho(770)^\pm\pi^\mp$ and the direct decay $\chi_{c2} \rightarrow \pi^+\pi^-\pi^0$, respectively, where the first uncertainties are statistical, and the second are systematic. Since the statistical significance for the $\chi_{c2} \rightarrow \rho(770)^\pm\pi^\mp$ is only 2.8σ , the upper limit at the 90% C.L. for the branching fraction is set to 1.2×10^{-5} by a Bayesian method, where the value is scaled with a factor $1/(1-\delta)$ which takes into account the effects of systematic uncertainties (δ).

The uncertainties from the branching fractions of $\psi(3686) \rightarrow \gamma\chi_{c2}$, $K_S \rightarrow \pi^+\pi^-$, $\pi^0 \rightarrow \gamma\gamma$, $a_2(1320) \rightarrow K\bar{K}$, and $K^* \rightarrow K\pi$ are quoted from the PDG [17]. The uncertainty on the number of $\psi(3686)$ events is about 0.8% [8, 9]. The uncertainties associated with the tracking and PID are 1% for every charged track [20]. The uncertainty related with EMC shower reconstruction efficiency is 1% per shower [20]. The uncertainties associated with the kinematic fit are estimated to be 0.5% and 0.6% for the 4C and 5C fit, respectively, by using a method to correct the charged-track helix parameters, as described in Ref. [21]. The uncertainty associated with the K_S reconstruction is estimated to be 2.5% [21]. The uncertainties related with the π^0 selection, the requirements on the π^0 recoil mass and the ω background veto (in $\chi_{c2} \rightarrow \rho(770)^\pm\pi^\mp$ mode only) are negligible.

In the decay $\chi_{c2} \rightarrow \rho(770)^\pm\pi^\mp$, the uncertainties due to the bin size and the fit range in the fit are estimated by repeating the fit with alternative bin sizes and fit ranges. The uncertainty due to the shape of $\chi_{c2} \rightarrow \pi^+\pi^-\pi^0$ is estimated by replacing the MC simulated line shape with a 3^{rd} polynomial function. The uncertainty due to the shape of the background is estimated by changing the χ_{c2} sideband regions. Assuming all the systematic errors are independent, the overall systematic associated with the fit is 10.3%, obtained by taking the quadrature sum of the individual values.

In the decay $\chi_{c2} \rightarrow K\bar{K}\pi$, the uncertainties due to the contribution from $K^*(1410)$ and $K^*(1680)$ are estimated by including these states in the fit. The uncertainties as-

sociated with the backgrounds are determined by changing the χ_{c2} and π^0 sideband regions. The spin density matrix corresponding to the $E1$ transition [14] is used in the nominal fit. To estimate the uncertainty, contributions from the quadrupole ($M2$) and other high order multipoles to the matrix [13] are included in the fit, and the changes in the final results are treated as a systematic uncertainty. The uncertainties associated with the resonance parameters of intermediate states are estimated by varying their values by 1σ of their uncertainties quoted in the PDG [17]. The uncertainty due to the barrier radius [12] when calculating $B_l(r)$ in Eq. (1) is estimated by alternative fits with $r = 0.25$ or 0.75 fm, respectively, where $r = 0.6$ fm is the nominal value. The uncertainty associated with the direct three-body decay $\chi_{c2} \rightarrow K\bar{K}\pi$ is estimated by alternative fits with other spin-parity hypotheses, *e.g.* a 0^- or 3^- non-resonant component in the $K\bar{K}$ or $K\pi$ systems. The largest changes in the signal yields are taken as systematic uncertainties.

In summary, the HSR suppressed processes of $\chi_{c2} \rightarrow K^*(892)\bar{K}$ and $\chi_{c2} \rightarrow \rho(770)^\pm\pi^\mp$ are studied with the $\psi(3686)$ data collected by BESIII for the first time. The branching fractions of $\chi_{c2} \rightarrow K^{\pm}(892)K^\mp$ and $\chi_{c2} \rightarrow K^{*0}(892)\bar{K}^0 + c.c.$ are measured to be $(1.5 \pm 0.1 \pm 0.2) \times 10^{-4}$ and $(1.3 \pm 0.2 \pm 0.2) \times 10^{-4}$, respectively, which are rather sizeable with respect to those of the HSR conserving decay $\chi_{c2} \rightarrow VV$ [17, 19]. These branching fractions are at least one order of magnitude larger than the upper limit of the branching fraction of $\chi_{c2} \rightarrow \rho(770)^\pm\pi^\mp$ (1.2×10^{-5}). It is worth noting that this phenomenon is anticipated by the HSR violation mechanism proposed in Ref. [7]. Namely, the HSR violation in $\chi_{c2} \rightarrow K^*(892)\bar{K}$ occurs via the intermediate meson loops due to the large U -spin symmetry breaking, while that in $\chi_{c2} \rightarrow \rho(770)^\pm\pi^\mp$ is due to isospin symmetry breaking. Due to the large mass difference between s and u/d quarks, the U -spin symmetry is broken more severely in comparison with isospin symmetry. This results in the larger decay branching for $\chi_{c2} \rightarrow K^*(892)\bar{K}$ than that for $\chi_{c2} \rightarrow \rho(770)^\pm\pi^\mp$. The results are crucial for further quantifying the HSR violation mechanisms [7] and also provide deeper insights into the underlying strong interaction dynamics in the charmonium energy region.

The BESIII collaboration thanks the staff of BEPCII and the IHEP computing center for their strong support. This work is supported in part by National Key Basic Research Program of China under Contract No. 2015CB856700; National Natural Science Foundation of China (NSFC) under Contracts Nos. 11175188, 11375205, 11425525, 11565006, 11521505, 11235011, 11322544, 11335008, 11425524, 11635010; the Chinese Academy of Sciences (CAS) Large-Scale Scientific Facility Program; the CAS Center for Excellence in Particle Physics (CCEPP); the Collaborative Innovation Center for Particles and Interactions (CICPI); Joint Large-Scale

Scientific Facility Funds of the NSFC and CAS under Contracts Nos. U1232201, U1332201; CAS under Contracts Nos. KJCX2-YW-N29, KJCX2-YW-N45; 100 Talents Program of CAS; National 1000 Talents Program of China; INPAC and Shanghai Key Laboratory for Particle Physics and Cosmology; German Research Foundation DFG under Contracts Nos. Collaborative Research Center CRC 1044, FOR 2359; Istituto Nazionale di Fisica Nucleare, Italy; Joint Large-Scale Scientific Facility Funds of the NSFC and CAS under Contract No. U1532257; Joint Large-Scale Scientific Facility Funds of the NSFC and CAS under Contract No. U1532258; Koninklijke Nederlandse Akademie van Wetenschappen (KNAW) under Contract No. 530-4CDP03; Ministry of Development of Turkey under Contract No. DPT2006K-120470; National Natural Science Foundation of China (NSFC) under Contract No. 11575133; NSFC under Contract No. 11275266; The Swedish Research Council; U. S. Department of Energy under Contracts Nos. DE-FG02-05ER41374, DE-SC-0010504, de-sc0012069; U.S. National Science Foundation; University of Groningen (RuG) and the Helmholtzzentrum fuer Schwerionenforschung GmbH (GSI), Darmstadt; WCU Program of National Research Foundation of Korea under Contract No. R32-2008-000-10155-0.

-
- [1] S. J. Brodsky and G. P. Lepage, Phys. Rev. D **24**, 2848 (1981).
 [2] V. L. Chernyak and A. R. Zhitnitsky, Nucl. Phys. B **201**,

- 492 (1982) [Erratum-ibid. B **214**, 547 (1983)].
 [3] V. L. Chernyak and A. R. Zhitnitsky, Phys. Rept. **112**, 173 (1984).
 [4] N. Brambilla *et al.* (Quarkonium Working Group), arXiv:hep-ph/0412158.
 [5] M. B. Voloshin, Prog. Part. Nucl. Phys. **61**, 455 (2008).
 [6] D. M. Asner *et al.* Int. J. of Mod. Phys. A **24** Supplement 1, (2009).
 [7] X. H. Liu and Q. Zhao, Phys. Rev. D **81**, 014017 (2010).
 [8] M. Ablikim *et al.* (BESIII Collaboration), Chin. Phys. C **37** 063001 (2013).
 [9] Using the same method as in Ref. [8], the number of $\psi(3686)$ for the 2012 data sample is determined to be $(341.1 \pm 2.1) \times 10^6$.
 [10] M. Ablikim *et al.* (BESIII Collaboration), Nucl. Instrum. Meth. A **614**, 345-399 (2010).
 [11] S. U. Chung, Phys. Rev. D **57**, 431 (1998); **48**, 1225 (1993).
 [12] B. S. Zou and D. V. Bugg, Eur. Phys. J. A **16**, 537 (2003).
 [13] M. Ablikim *et al.* (BESIII Collaboration), Phys. Rev. D **84**, 092006 (2011).
 [14] G. Karl, J. Meshkov and J. L. Rosner, Phys. Rev. D **13**, 1203 (1976).
 [15] F. James, CERN Program Library Long Writeup D 506 (1998).
 [16] M. Ablikim *et al.* (BESIII Collaboration), Phys. Rev. D **86**, 072011 (2012).
 [17] K. A. Olive *et al.* (Particle Data Group), Chin. Phys. C **38**, 090001 (2014).
 [18] G. D'Agostini, Nucl. Instrum. Meth. A **346**, 306 (1994).
 [19] M. Ablikim *et al.* (BESIII Collaboration), Phys. Rev. Lett. **107**, 092001 (2011).
 [20] M. Ablikim *et al.* (BESIII Collaboration), Phys. Rev. D **83**, 112005 (2011).
 [21] M. Ablikim *et al.* (BESIII Collaboration), Phys. Rev. D **87**, 012002 (2013).